ACS APPLIED NANO MATERIALS
Cite This: ACS Appl. Nano Mater. 2019, 2, 5809−5816
Article
www.acsanm.org

Mimicking Polymer Surfaces Using Cyclohexyl- and Perfluorocyclohexyl-Terminated Self-Assembled Monolayers

Tianlang Yu, Maria D. Marquez, Oussama Zenasni, and T. Randall Lee*

Department of Chemistry and the Texas Center for Superconductivity, University of Houston, 4800 Calhoun Road, Houston, Texas 77204-5003, United States

Supporting Information

ABSTRACT: This article describes the synthesis of two cyclohexyl-terminated alkanethiols (**HCyHnSH**; n = 10 and 11) and their fluorinated analogs $C_6F_{11}(CH_2)_nSH$ (n = 10 and 11; **FCyHnSH**). These ring-terminated adsorbates were used to generate self-assembled monolayers (SAMs) on gold surfaces to serve as model polymeric interfaces on metal substrates. The corresponding SAMs were characterized using ellipsometry, X-ray photoelectron spectroscopy (XPS), polarization modulation infrared reflection−absorption spectroscopy (PM-IRRAS), and contact angle goniometry. While the ellipsometric thicknesses were consistent with monolayer formation, analysis by XPS indicated that the **HCyHnSH** SAMs exhibited greater packing densities than their fluorocarbon analogs. However, PM-IRRAS spectra revealed that the underlying methylene units in the **HCyHnSH** SAMs were less conformationally ordered than their fluorocarbon analogs. In all the characterizations, no discernible "odd−even" effect was observed in either the **HCyHnSH** or the **FCyHnSH** SAMs, plausibly due to the bulkiness and conformational flexibility of the chain termini. Interestingly, comparison of the contact angles of a wide range of contacting liquids on these SAMs and their polymeric analogs, polyethylene (PE) and polytetrafluoroethylene (PTFE), found that these liquids exhibited similar wettability on the **HCyHnSH** SAMs and PE surfaces, and separately on the **FCyHnSH** SAMs and PTFE surfaces. These results suggest that these SAMs can successfully act as mimics of nanoscale polymer films and can be used in future studies (e.g., ion-surface collisions and plasma modification) without concerns of surface reconstruction.

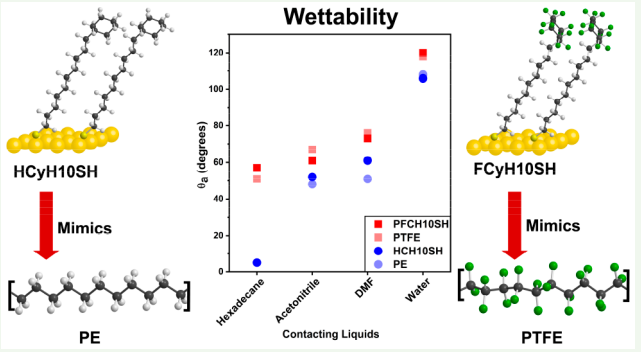

KEYWORDS: *self-assembled monolayers (SAMs), polymer mimics, wettability, surface reconstruction, polymer surfaces*

INTRODUCTION

Polymer coatings are widely used as protective layers in industrial settings for devices working under a wide range of conditions.[1] The flexibility, ease of application, and their lightweight properties render polymer coatings attractive for use as a protective layer on various types of surfaces to protect against corrosion and/or mechanical damage.[2] The most commonly used polymers for coatings in industry are polyethylene (PE) and polytetrafluoroethylene (PTFE). Since its discovery in 1941,[3] PTFE has been used in diverse applications due to its excellent properties, which include low surface friction,[2] high chemical and thermal stability,[4] high hydrophobicity, and oleophobicity;[5] these characteristics have allowed PTFE to become the candidate of choice in certain coating applications.[6] Regarding the microstructure of PTFE, the polymer chains adopt two types of morphologies that coexist: crystalline and amorphous.[7,8] In the crystalline region of PTFE, the helical chains align themselves parallel to each other, while in the amorphous region, their arrangement is random.[9,10] Crystalline PTFE undergoes rapid and complicated phase transitions near room temperature.[11,12] Compared to rigid materials, such as inorganic crystals, polymers behave more like viscous liquids than solids due to the relatively weak van der Waals interactions between the polymer chains.[13] This characteristic is particularly true for PTFE, as PTFE exhibits significant wear under sliding conditions and cold-flow behavior under stress.[2,14]

To construct nanoscale PE and PTFE thin films, an understanding of the microstructure of polymeric interfaces becomes essential in coating applications. Among the numerous analytical techniques available, the measurement of contact angles is an inexpensive tool for investigating the interfacial properties of organic thin films.[15,16] In a common coating method, small particles of the polymer are sprayed onto an uncoated surface followed by sintering to form a polymer film.[17] However, it is difficult to control the homogeneity of polymer surfaces on the nanoscale. In addition to being rough, polymer surfaces are sensitive to surface reconstruction under changing conditions.[18] When a liquid is in contact with a polymer surface, the liquid can intercalate

Received: July 4, 2019
Accepted: August 26, 2019
Published: August 26, 2019

DOI: 10.1021/acsanm.9b01268
ACS Appl. Nano Mater. 2019, 2, 5809−5816

between the polymer chains and cause reconstruction of the surface, also known as swelling.[19] Polymers that swell under the influence of a contacting liquid exhibit a decrease in the contact angle and an increase in the hysteresis value.[20,21] Notably, the study of structure−property relationships of polymeric surfaces, particularly for nanotribology purposes, continues to receive attention. The aforementioned shortcomings and the continuing miniaturization of devices are driving the need to develop an ideal model to better understand polymer interfaces, without surface reconstruction, and subsequently the development of improved nanoscale low friction polymer coatings.[22−24]

Since Nuzzo and Allara published their work on the monolayer assembly of organic adsorbates on gold substrates,[25] self-assembled monolayers (SAMs) have been used in a variety of fields, including corrosion prevention,[26] electronic applications,[27] microelectromechanical systems (MEMS) devices,[28] biomaterial coatings,[29] and biosensors.[30] Researchers have also used SAMs as model systems to investigate structure−property relationships due to the ability to synthetically alter the adsorbate to impart selected packing densities or expose specific terminal functionalities.[31] For example, the Wysocki group utilized ion-surface collisions to characterize organic thin films derived from alkyl- and fluoroalkyl-terminated SAMs on gold.[32] Moreover, the ability to tailor the terminal functionality of an adsorbate allowed for the use of fluorinated SAMs (FSAMs) to generate functionalized surfaces with low wettability and coefficients of friction.[33−36] In related work, Barriet and co-workers used cyclopropyl-terminated SAMs to mimic the structural and interfacial properties (i.e., wettability) of polyethylene (PE)-based films.[37] The resemblance in the wettability data of cyclopropyl-terminated SAMs and PE-based surfaces provided insight into the relationship between the interfacial properties and nanostructure of polymer interfaces.

In the present study, we designed cyclohexyl- and perfluorocyclohexyl-terminated monolayer films on gold to serve as mimics to the surfaces of the commercially relevant polymers PE and PTFE, respectively. These films were generated from cyclohexyl-terminated alkanethiols (**HCyHnSH**; n = 10 and 11) and their fluorocarbon analogs $C_6F_{11}(CH_2)_nSH$ (n = 10 and 11; **FCyHnSH**) (see Figure 1). This study is based on the premise that **HCyHnSH**-based films would expose an interface comprised of CH_2 groups, which can mimic the surface/backbone of PE films; conversely, we anticipated that **FCyHnSH**-based films would expose an interface comprised of CF_2 groups, which can mimic the surface/backbone of PTFE films (see Scheme 1).

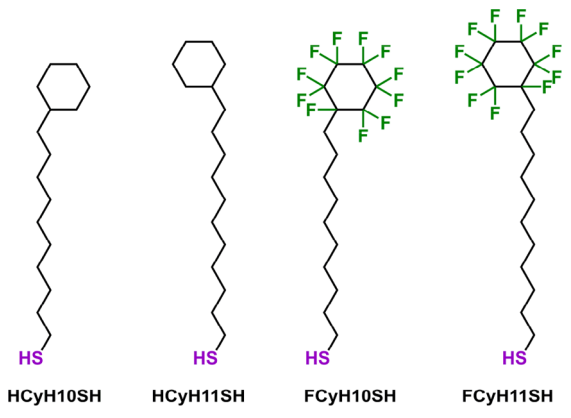

Figure 1. Molecular structures of the cyclohexyl-terminated thiols used in this study.

Studies of these films will allow us to evaluate the interfacial properties of solely CH_2 and CF_2 termini, which closely resemble polymeric backbones, without the facile surface reconstruction found in polymer-based films. Importantly, the **FCyHnSH** SAMs offer a rare system in which the van der Waals forces of CF_2-based interfaces can be unambiguously evaluated. Prior studies of fluorinated SAMs and related thin films have been limited to systems in which the interface is comprised in whole or in part by CF_3 moieties, which are quite distinct from PTFE-based surfaces.[33,35,38,39] Additionally, we envisioned that the permanent dipole at the FC-HC junction in **FCyHnSH** SAMs would be buried underneath the bulky perfluorocyclohexyl group, which would eliminate its effects on the interfacial energy of the SAM,[33,38,39] rendering this system similar to the surface of PTFE. Furthermore, the cyclohexane terminus suffers from little ring strain and is more flexible than our previously studied cyclopropyl system,[37] which allows all carbon atoms in the cyclohexyl system to adopt sp^3 hybridization as in linear PE chains. Similarly, and given the synthetic challenges associated with the perfluorocyclopropyl group, we chose the perfluorocyclohexyl tailgroup to generate CF_2 interfaces. As a whole, these considerations compelled us to pursue SAMs with cyclohexyl termini to model and study PE and PTFE surfaces.

In this study, ellipsometry (to evaluate the thickness of the films), X-ray photoelectron spectroscopy (XPS, for elemental analysis), and polarization modulation reflection−absorption infrared spectroscopy (PM-IRRAS, to evaluate the orientation and conformational order of the films) were used to characterize the investigated SAMs formed from the cyclohexyl-terminated adsorbates and octadecanethiol (**H18SH**), which served as a reference standard. The interfacial wettability of the SAMs, PE, and PTFE films were characterized using contact angle measurements.

EXPERIMENTAL PROCEDURES

Materials and chemicals used, details of the synthetic procedures (Supporting Information (SI) Schemes S1 and S2), spectroscopic characterization data for the **HCyHnSH** and **FCyHnSH** adsorbates (^1H, ^{19}F, and ^{13}C NMR spectra shown in SI Figures S1−S10), preparation of the Au substrates used in the investigation, and instrumental methods used are described in the SI.

RESULTS AND DISCUSSION

Ellipsometric Thickness Measurements. Table 1 displays the average ellipsometric thickness measurements of the investigated SAMs on gold. The average thickness of the **H18SH** SAM was 22 Å, which is consistent with the value in the literature.[40] Data for the **H18SH** adsorbate serve as a reference standard to ensure the quality and reliability of the evaporated Au substrates used in the study.

Separately, the ellipsometric thickness values for the **HCyHnSH** SAMs having 10 and 11 methylene groups are within the experimental error, ∼14−15 Å. The same trend was also observed for the **FCyHnSH** SAMs, where molecules bearing 10 backbone methylene units have a thickness of ∼13 Å and those with 11 hydrocarbons have a thickness of ∼12 Å. The high similarity of the monolayer thicknesses, regardless of the size of the underlying hydrocarbon spacer, might be due to the hydrocarbon chains adopting a trans-

DOI: 10.1021/acsanm.9b01268
ACS Appl. Nano Mater. 2019, 2, 5809−5816

Scheme 1. Illustration of the Investigated SAMs, HCyHnSH (Left) and FCyHnSH (Right), on Gold That Mimic PE and PTFE Interfaces

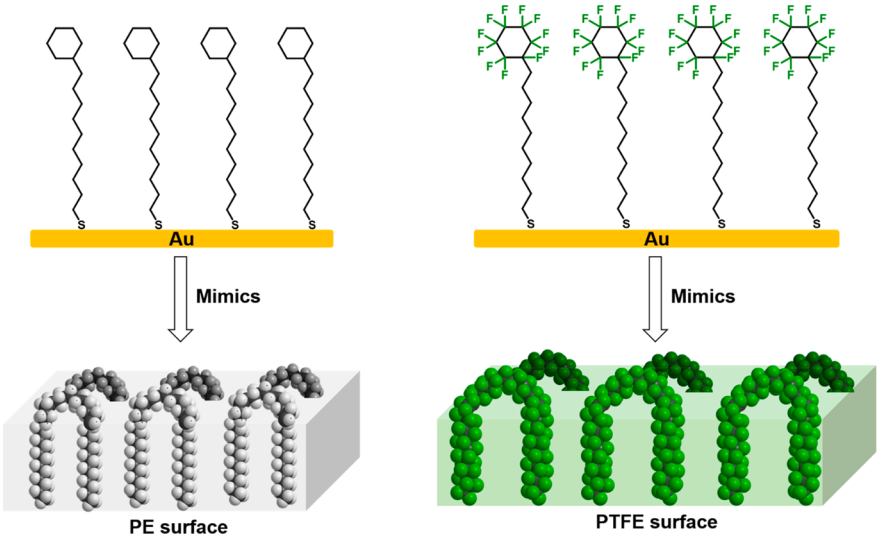

Table 1. Ellipsometric Thicknesses of the H18SH, HCyHnSH, and FCyHnSH SAMs

adsorbate	thickness (Å)
H18SH	22 ± 1
HCyH10SH	15 ± 1
HCyH11SH	14 ± 1
FCyH10SH	13 ± 1
FCyH11SH	12 ± 1

extended conformation to maximize interchain van der Waals forces, which leads to similar packing densities in the fluorocarbon or hydrocarbon films.[40] Yet, we notice that the **HCyHnSH** SAMs showed a slightly greater thickness than the **FCyHnSH** SAMs, Table 1. The observed slightly lower thickness for the **FCyHnSH** SAMs might arise from a lower number of molecules per unit area in the fluorinated SAMs as compared to the hydrocarbon analogs. The van der Waals diameter of fluorine is 1.47 Å, which is larger than hydrogen (1.20 Å), leading to bulkier termini in the **FCyHnSH** SAMs.[41−43] Another possible reason for such a reduction might arise from the fluorinated films being more tilted than their hydrocarbon counterparts, which can also be attributed to the larger chain termini in the fluorinated films. We note also that the low thicknesses of the **FCyHnSH** SAMs can plausibly be attributed to the use of a refractive index of 1.45 when measuring the ellipsometric thickness of partially fluorinated organic films, as noted previously.[44,45] Further analysis of the packing densities and conformational order of the chains in these films is detailed below in the XPS and PM-IRRAS sections, respectively.

Analysis of the Chemical Composition of the Films Using XPS. In analyses of organic thin films, XPS is a commonly used technique for determining (1) the chemical composition of organic films, (2) the oxidation state of elements, (3) the nature of the bonding of adsorbates on surfaces, and (4) the relative chain packing densities of organic films.[46,47] Figure 2 shows the XPS spectra of the binding

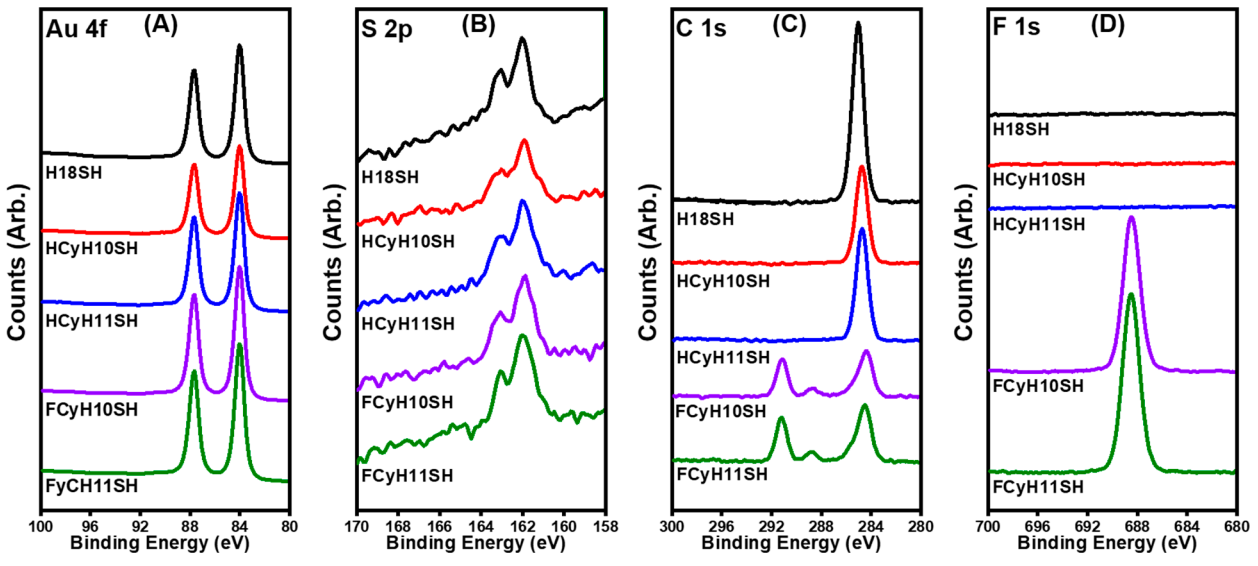

Figure 2. XPS spectra of the (A) Au 4f, (B) S 2p, (C) C 1s, and (D) F 1s binding regions of the SAMs.

DOI: 10.1021/acsanm.9b01268
ACS Appl. Nano Mater. 2019, 2, 5809−5816

regions of the Au 4f, S 2p, C 1s, and F 1s core electrons, respectively. The precise binding energies of the peaks in the spectra are provided in Table S1 in the Supporting Information. Figure 2A shows the expected peaks for Au 4f in all of the SAMs. Spectra of the S 2p region, shown in Figure 2B, can be used to evaluate the binding of the thiol-based adsorbates to the Au surface.[48−50] The spectra in Figure 2B exhibit a characteristic peak with spin−orbit splitting, which manifests as a doublet and is attributed to S $2p_{3/2}$ (~162.0 eV) and S $2p_{1/2}$ (163.0 eV). The peak appeared for all of the SAMs analyzed in the study and is consistent with the presence of bound thiolate.[49,50] Moreover, the absence of peaks at ~164 or 166 eV and higher binding energy suggests the absence of unbound or highly oxidized sulfur species, respectively, in the investigated SAMs. Figure 2C shows the XPS spectra for the C 1s region; the peak positions are given in Table 2. For the

Table 2. Relative Chain Packing Densities of SAMs and XPS Binding Energies of C 1s (eV)

adsorbate	C 1s (CH_2) (eV)	C 1s (CF) (eV)	C 1s (CF_2) (eV)	relative packing density (%)
H18SH	285.0			100
HCyH10SH	284.7			72 ± 5
HCyH11SH	284.7			71 ± 8
FCyH10SH	284.4	288.6	291.1	64 ± 6
FCyH10SH	284.5	288.7	291.1	63 ± 6

H18SH reference SAM, one peak with a binding energy of 285.0 eV was apparent, which we attribute to all of the carbons with attenuation of the carbon directly attached to sulfur.[49] The XPS spectra of the **HCyHnSH** SAMs exhibited one peak at 284.7 eV, which indicates all of the C 1s electrons arise from the carbons of the cyclohexyl ring, the tertiary carbon attached to the alkyl chain, and the carbons of the alkyl chain. In contrast, the C 1s spectra of the **FCyHnSH** SAMs revealed two large peaks that can be attributed to the CH_2 and CF_2 units at ~284.4 eV and ~291.1 eV, respectively, with a small broad peak in between (~288.6 eV). We believe that the broad peak at ~288.6 eV corresponds to the CF carbon of the perfluorinated cyclohexyl ring attached to the alkyl chain, which is expected to have a lower binding energy than the more highly fluorinated CF_2 carbons.[51] As for the F 1s region, the **FCyHnSH** SAMs both exhibited a sharp peak at 688.4 eV, while the other SAMs showed no peaks in the F 1s region, which is consistent with the chemical structures of the adsorbates.

A quantitative analysis of the relative packing density can also be obtained from the XPS spectra. To evaluate the relative chain packing densities in the SAMs, we utilized the integrated intensities of the S 2p and Au 4f core electrons from the XPS spectra to calculate the S/Au ratio.[52] In our analysis, the **H18SH** SAM was used as a reference for a system with 100% chain packing density. Further, since photoelectrons are attenuated the same in hydrocarbon and fluorocarbon SAMs on gold,[53] the packing densities of all SAMs were calculated in the same manner. Table 2 shows the relative chain packing densities of all of the investigated SAMs.

Note that for cyclohexyl SAMs within the same series (i.e., for SAMs derived from **HCyHnSH** or **FCyHnSH**), all adsorbates adopted similar packing densities regardless of the length of the methylene spacer. For example, the packing densities of the **HCyH10SH** and **HCyH11SH** SAMs were 72% and 71%, respectively, while the **FCyH10SH** and **FCyH11SH** SAMs exhibited packing densities of 64% and 63%, respectively. Moreover, the data also show that the packing densities of the **HCyHnSH** SAMs were greater than those of the **FCyHnSH** SAMs. Such discrepancies are consistent with the progressive increase in the size of the chain termini in the **H18SH**, **HCyHnSH**, and **FCyHnSH** SAMs. Compared to the **H18SH** monolayers, the **HCyHnSH** SAMs have larger terminal groups, which reduces the relative packing densities of the chains to ~72%. This effect is further augmented in the **FCyHnSH** SAMs, where the perfluorocyclohexyl termini leads to a reduction in the relative packing densities of these films to ~64%. This latter decrease is plausibly due to the increase in the van der Waals (vdW) volume of the chain termini after the replacement of hydrogen atoms (vdW radius of 1.20 Å) with fluorine atoms (vdW radius of 1.47 Å),[42] which makes perfluorinated cyclohexyl tailgroups more sterically bulky (and more rigid) than their hydrocarbon analogs.

The C 1s binding energy region can also be used to provide a qualitative assessment of the relative packing density for a series of structurally similar SAMs.[54] The values of the binding energy of the C 1s core electrons generated from the CH_2 units corroborates the above-mentioned analysis of changes in the relative packing densities as a function of terminal group size. The binding energies of the C 1s electrons originating from the CH_2 decrease with an increase in the size of the chain termini. For example, the binding energy of C 1s electrons decreased from 285.0 for the **H18SH** SAM to 284.7 eV for the **HCyHnSH** SAMs. Similarly, the aliphatic C 1s binding energy for the **FCyHnSH** SAMs decreased further to ~284.4 eV. This phenomenon arises due to a final state effect, where positive charges generated from the photoelectron emission are easily screened in films with lower packing densities (i.e., weaker insulators) than in densely packed films, which gives rise to an increase in the energy required to eject electrons from the latter films.[47] For the SAMs within a series (i.e., **HCyH10SH** and **HCyH11SH** vs **FCyH10SH** and **FCyH11SH**), there was no observable difference in the binding energies, indicating the chain length of the spacer has no effect on the packing density of the films. In summary, evaluation of the C 1s binding energies of these films shows that the packing densities decrease in the following order: **H18SH** > **HCyHnSH** > **FCyHnSH**, which is consistent with the observed S/Au ratios.

Assessment of Chain Conformational Order Using PM-IRRAS. IR spectroscopy of surfaces has proven to be a valuable tool for probing the relative conformational order and orientation of molecules within a SAM.[55] In particular, the position of the methylene antisymmetric stretching band ($\nu_{as}^{CH_2}$) of the hydrocarbon backbone can be used to evaluate the conformational order (i.e., crystalline nature).[56] Figure 3 shows the PM-IRRAS spectra for the C−H stretching region of the current set of SAMs.

Table 3 presents the precise peak assignments (cm^{-1}) in the PM-IRRAS spectra of the current set of SAMs. For well-ordered alkanethiol monolayers, such as the **H18SH** SAM, the $\nu_{as}^{CH_2}$ stretch has been assigned at 2918 cm^{-1}, which indicates a trans-extended crystalline conformation.[56] However, these bands tend to blue shift in the case of poorly ordered (liquid-like) SAMs.[57] For the purpose of peak assignment, deconvoluted spectra of the **HCyHnSH** SAMs are provided in the Supporting Information (see SI Figure S11). For the **HCyHnSH** series, we observed a consistent positioning of the $\nu_{as}^{CH_2}$ stretch (2923−2924 cm^{-1}), regardless of chain length,

DOI: 10.1021/acsanm.9b01268
ACS Appl. Nano Mater. 2019, 2, 5809−5816

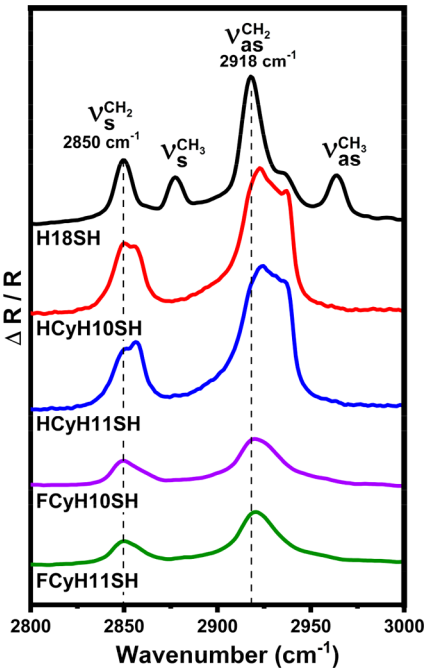

Figure 3. PM-IRRAS spectra showing the C−H stretching region of the **H18SH**, **HCyHnSH**, and **FCyHnSH** SAMs.

Table 3. Peak Assignments (cm^{-1}) for the PM-IRRAS Spectra of the H18SH, HCyHnSH, and FCyHnSH SAMs

adsorbate	$\nu_s^{CH_2}$(cm^{-1})	$\nu_s^{CH_3}$(cm^{-1})	$\nu_{as}^{CH_2}$(cm^{-1})	$\nu_{as}^{CH_3}$(cm^{-1})
H18SH	2850	2877	2918	2964
HCyH10SH	2850 (2858 ring)		2924 (2937 ring)	
HCyH11SH	2851 (2857 ring)		2923 (2937 ring)	
FCyH10SH	2849		2920	
FCyH11SH	2850		2921	

for both the **HCyH10SH** and **HCyH11SH** SAMs, which is in agreement to analogously structured phosphonic acid SAMs on metal oxide surfaces.[58] In addition, we observed broadening of both $\nu_s^{CH_2}$ and $\nu_{as}^{CH_2}$ peaks in the spectra, which might be due to an overlap between the peaks of the methylene units of the alkyl chain and those in the cyclohexane ring. Furthermore, the PM-IRRAS spectra of the **FCyH10SH** and **FCyH11SH** SAMs also displayed similar characteristics despite the difference in the hydrocarbon chain length. The $\nu_{as}^{CH_2}$ of the **FCyHnSH** SAMs was located at ~2920 cm^{-1}, which indicates that the methylene chains of the fluorinated SAMs are slightly more ordered than their hydrocarbon analogs.

Contact Angle Measurements. The interfacial properties of the investigated SAMs and their polymer counterparts (PE and PTFE) were probed using a variety of contacting liquids ranging from polar protic (water, W, γ_{LV} = 72.0 mN/m; formamide, FA, γ_{LV} = 58.2 mN/m; and methyl formamide, MF, γ_{LV} = 38.0 mN/m), to polar aprotic (dimethylformamide, DMF, γ_{LV} = 37.1 mN/m; and acetonitrile, ACN γ_{LV} = 29.3 mN/m), and nonpolar aprotic (squalane, SQ, γ_{LV} = 28.9 mN/m; and hexadecane, HD γ_{LV} = 27.5 mN/m) liquids.[59,60] Table 4 lists the advancing contact angles (ACAs) and the hysteresis values (difference between advancing and receding contact angles) for all probe liquids employed on the **H18SH**, **HCyHnSH**, **FCyHnSH**, **PE**, and **PTFE** surfaces. Optical images of the advancing contact angles for all surfaces and liquids analyzed are provided in Figures S11−S17 in the Supporting Information.

Figure 4 compares the ACA values obtained for all the liquids on the investigated SAMs and the two polymer surfaces. The wettability data of the **H18SH** SAMs, PE, and PTFE agree with previously reported values.[5,36,54] Furthermore, the wettability data for these liquids on both the **FCyHnSH** and **HCyHnSH** series showed no clear evidence for an "odd−even" effect. Overall, the wettability data for all SAMs resemble those of the polymers they were designed to

Table 4. Advancing Contact Angles (θ_a, °) of the Investigated SAMs and Polymers Using Various Probe Liquids[a]

	W	FA	MF	DMF	ACN	SQ	HD
H18SH	117 (5)	99 (7)	80 (7)	74 (6)	68 (8)	58 (8)	47 (7)
HCyH10SH	106 (6)	85 (7)	67 (8)	61 (6)	52 (7)	16 (−)	<10 (−)
HCyH11SH	107 (6)	86 (7)	68 (7)	60 (4)	51 (7)	15 (−)	<10 (−)
PE	108 (10)	85 (10)	58 (12)	51 (8)	48 (9)	20 (−)	<10 (−)
FCyH10SH	120 (7)	103 (7)	82 (10)	73 (6)	61 (4)	64 (9)	57 (8)
FCyH11SH	119 (8)	104 (7)	80 (10)	72 (5)	63 (4)	66 (10)	59 (7)
PTFE	118 (14)	102 (22)	81 (15)	76 (12)	67 (12)	60 (21)	46 (23)

[a]Entries marked (−) reflect receding contact angles <10° (commonly defined as fully wettable). Values of hysteresis ($\theta_a - \theta_r$, °) are given in parentheses.

DOI: 10.1021/acsanm.9b01268
ACS Appl. Nano Mater. 2019, 2, 5809−5816

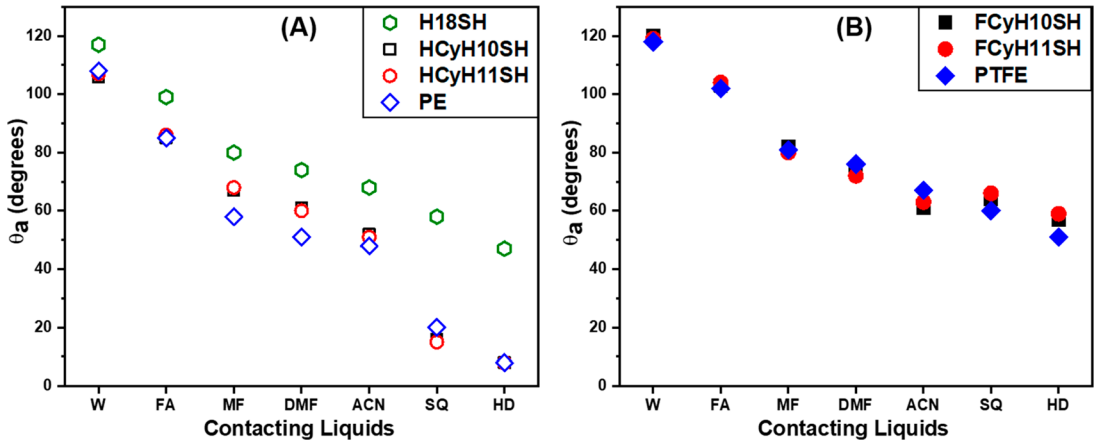

Figure 4. Comparison of the advancing contact angles of various probe liquids for: (A) the **HCyHnSH** SAMs and **PE**; (B) the **FCyHnSH** SAMs and **PTFE**. W = water; *F* = formamide; MF = methylformamide; DMF = dimethylformamide; ACN = acetonitrile; SQ = squalane; HD = hexadecane. HD fully wets the **HCyHnSH** SAMs and **PE**. The **H18SH** SAM is included as a reference. *Error bars that are not visible fall within the symbols.*.

mimic. For example, the ACA of water on the **HCyHnSH** SAMs, 106−107°, was similar to the ACA of water on PE, 108°. Similarly, water exhibited comparable contact angle values on the **FCyHnSH** SAMs, 119−120°, as on the PTFE surface, 118°. Importantly, the PE surface swelled quickly upon contact with MF, DMF, ACN, SQ, and HD, indicating that these liquids intercalate into the PE surface, leading to reorganization of the polymer chains. To compare the ACAs of PE with those of the **HCyHnSH** SAMs, all contact angle data taken on the **PE** surfaces were collected within 5 s of coming into contact with the above-mentioned liquids. In contrast, we observed no significant changes in the contact angles on the **PTFE** as a function of time of contact with the liquids, which is consistent with previous wettability studies of **PTFE**.[20] Similarly, the contact angles for all liquids on the **HCyHnSH** and **FCyHnSH** SAMs were constant over time, suggesting no surface reorganization.

All of the surfaces examined showed an increasing trend in wettability (i.e., decrease in contact angle) as the surface tension of the liquid decreased, save for one exception involving acetonitrile and squalene on the **FCyHnSH** SAMs (vide infra). Water, with the highest surface tension (γ_{LV} = 71.97 mN/m), showed the highest contact angle on all the surfaces followed by formamide, methylformamide, dimethylformamide, acetonitrile, squalane, and hexadecane. As the intermolecular forces within the liquid decrease (i.e., hydrogen bonding and van der Waals forces), self-association of the contacting liquid also decreases, leading to increased interactions with the interface (i.e., a lower contact angle and thus a more wettable surface).[61] Accordingly, among the polar contacting liquids, water interacts the least with these surfaces due to its high surface tension (γ_{LV} = 71.97 mN/m) and the absence of hydrogen bonding with the surface and the absence of oriented dipoles near the interface.[32,37,38,43] Note that the ACA values of water on the fluorinated surfaces were higher than those on the hydrocarbon ones, which supports our earlier hypothesis that the size of the perfluorinated cyclohexyl ring would sufficiently screen and thereby mitigate any effects due to FC-HC dipole at the ring-alkyl chain junction.

Both squalane and hexadecane are nonpolar liquids with similar surface tensions (28.9 mN/m for squalane and 27.5 mN/m for hexadecane), which interact with all the investigated surfaces exclusively through dispersive (van der Waals) interactions. And although acetonitrile is polar, its surface tension (ACN γ_{LV} = 29.3 mN/m) is comparable to those of the nonpolar liquids. This rather small difference in liquid surface tension might be responsible for the minor discrepancy noted above (i.e., the **FCyHnSH** SAMs were less wettable by squalane than by acetonitrile). We note, however, that for the investigated PTFE sample, the wettability trends followed the expected trajectory.

Separately, the **HCyHnSH** SAMs and PE surfaces were more wettable by all contacting liquids than the reference **H18SH** SAM. The observed differences in the wettability are a result of the interfacial features of the films. In the **HCyHnSH** and **PE** surfaces there is an increase in atomic contact per unit area compared to the **H18SH** SAM.[52,63] The chain termini in the **H18SH** SAM are separated by a distance of ∼5.0 Å.[44] However, the distance between the CH_2 units of the cyclohexyl rings and the PE chain is the same as the length of a C−C bond, ∼1.54 Å,[62] which can plausibly give rise to stronger vdW interactions between the interface and the nonpolar contacting liquids.[52,63]

The wettability data presented in Figure 4 shows that the current set of SAMs offers a suitable model for evaluating the interfacial properties of the PE and PTFE polymers. Both pure PE and PTFE are semicrystalline polymers at room temperature, where their crystalline regions are composed of planes of parallel linear chains.[9,64] However, the sliding movement between the different planes and reorientation of the polymer chains make the direct analysis of these polymer interfaces a challenging task. Separately, the observed agreement between the wettability data of the **FCyHnSH** and **HCyHnSH** SAMs with their corresponding polymer films indicate that these surfaces have a similar density of interfacial atomic contacts. Furthermore, the measurements of hysteresis, which can be affected by surface roughness and/or surface reconstruction, indicate that the hysteresis values for the investigated SAMs are smaller than those for the polymer surfaces (see Table 4). As such, the investigated SAM surfaces have lower surface roughness/heterogeneity compared to the surfaces of the two polymers, which is consistent with the absence of surface reconstruction in the SAM films.

DOI: 10.1021/acsanm.9b01268
ACS Appl. Nano Mater. 2019, 2, 5809−5816

CONCLUSIONS

Adsorbates for generating cyclohexyl-terminated SAMs (**HCyHnSH**) and perfluorocyclohexyl-terminated SAMs (**FCyHnSH**) were synthesized and used to form monolayers on gold that serve as interfacial polymer mimics on metal substrates. The monolayer films were characterized using ellipsometry, XPS, PM-IRRAS, and contact angle measurements. Analysis by XPS indicated that the **FCyHnSH** SAMs exhibited lower packing densities than their hydrocarbon analogs, and both types of SAMs exhibited lower packing densities than the **H18SH** films, which correlated with the steric bulk of the chain termini in these SAMs. The PM-IRRAS spectra showed that the chain backbones of both **FCyHnSH** and **HCyHnSH** SAMs were less conformationally ordered than normal hydrocarbon analogs. Furthermore, the **HCyHnSH** SAMs exhibited wettabilities similar to PE, while their fluorocarbon analogs exhibited wettabilities similar to **PTFE** for a wide range of contacting liquids with no evidence of surface reconstruction in the SAMs. Therefore, SAMs on gold derived from cyclohexyl-terminated thiols can thus serve as robust models to study the interfacial properties and reactivities of polymer surfaces.

ASSOCIATED CONTENT

Supporting Information

The Supporting Information is available free of charge on the ACS Publications website at DOI: 10.1021/acsanm.9b01268.

Details of the materials used and the synthetic procedures (Schemes S1 and S2) for the **HCyHnSH** and **FCyHnSH** adsorbates, including their characterization by ^{1}H, ^{19}F, and ^{13}C NMR (Figures S1−S10); Instrumental procedures and the preparation of the Au substrates used in the study; Addtional XPS data, deconvoluted PM-IRRAS spectra of the **HCyHnSH** SAMs (Figure S11), and optical images of all contact angles taken on the surfaces (Figures S12−S18)(PDF)

AUTHOR INFORMATION

Corresponding Author

*E-mail: trlee@uh.edu.

ORCID

T. Randall Lee: 0000-0001-9584-8861

Notes

The authors declare no competing financial interest.

ACKNOWLEDGMENTS

We are grateful for the generous support from the National Science Foundation (CHE-1710561), the Robert A. Welch Foundation (E-1320), and the Texas Center for Superconductivity at the University of Houston.

REFERENCES

(1) Bishop, C. A. Chapter 11 - Polymer Coating Basic Information. In *Vacuum Deposition onto Webs, Films and Foils*, 3rd ed.; Bishop, C. A., Ed.; William Andrew Publishing: Boston, 2015; pp 221−239.

(2) Grainger, D. W.; Stewart, C. W. Fluorinated Coatings and Films: Motivation and Significance. *ACS Symp. Ser.* **2001**, *787*, 1−14.

(3) Plunkett, R. J. Tetrafluoroethylene Polymers. U.S. Patent 2,230,654, February 4, 1941.

(4) Patrick, C. R. Thermal Stability of Polytetrafluoroethylene. *Nature* **1958**, *181*, 698−698.

(5) Lee, S.; Park, J. S.; Lee, T. R. The Wettability of Fluoropolymer Surfaces: Influence of Surface Dipoles. *Langmuir* **2008**, *24*, 4817−4826.

(6) Jones, B. Fluoropolymers for Coating Applications. *J. Coat. Technol. Res.* **2008**, *5*, 44−48.

(7) Yamamoto, T. Computer Modeling of Polymer Crystallization − toward Computer-Assisted Materials' Design. *Polymer* **2009**, *50*, 1975−1985.

(8) Brown, E. N.; Rae, P. J.; Dattelbaum, D. M.; Clausen, B.; Brown, D. W. In-Situ Measurement of Crystalline Lattice Strains in Polytetrafluoroethylene. *Exp. Mech.* **2008**, *48*, 119−131.

(9) Brown, E. N.; Dattelbaum, D. M. The Role of Crystalline Phase on Fracture and Microstructure Evolution of Polytetrafluoroethylene (PTFE). *Polymer* **2005**, *46*, 3056−3068.

(10) Brown, E. N.; Trujillo, C. P.; Gray, G. T.; Rae, P. J.; Bourne, N. K. Soft Recovery of Polytetrafluoroethylene Shocked through the Crystalline Phase II-III Transition. *J. Appl. Phys.* **2007**, *101*, 024916.

(11) Clark, E. S. The Molecular Conformations of Polytetrafluoroethylene: Forms Ii and Iv. *Polymer* **1999**, *40*, 4659−4665.

(12) Bunn, C. W.; Howells, E. R. Structures of Molecules and Crystals of Fluoro-Carbons. *Nature* **1954**, *174*, 549−551.

(13) Schrauwen, B. A. G.; Janssen, R. P. M.; Govaert, L. E.; Meijer, H. E. H. Intrinsic Deformation Behavior of Semicrystalline Polymers. *Macromolecules* **2004**, *37*, 6069−6078.

(14) Allam, I. M. Solid Lubricants for Applications at Elevated-Temperatures - a Review. *J. Mater. Sci.* **1991**, *26*, 3977−3984.

(15) Zhang, X.; Shi, F.; Niu, J.; Jiang, Y. G.; Wang, Z. Q. Superhydrophobic Surfaces: From Structural Control to Functional Application. *J. Mater. Chem.* **2008**, *18*, 621−633.

(16) Yuan, Y.; Lee, T. R. Contact Angle and Wetting Properties. In *Surface Science Techniques*; Bracco, G., Holst, B., Eds.; Springer Berlin Heidelberg: Berlin, Heidelberg, 2013; pp 3−34.

(17) Andena, L.; Rink, M.; Polastri, F. Simulation of PTFE Sintering: Thermal Stresses and Deformation Behavior. *Polym. Eng. Sci.* **2004**, *44*, 1368−1378.

(18) Holmes-Farley, S. R.; Bain, C. D.; Whitesides, G. M. Wetting of Functionalized Polyethylene Film Having Ionizable Organic Acids and Bases at the Polymer-Water Interface: Relations between Functional Group Polarity, Extent of Ionization, and Contact Angle with Water. *Langmuir* **1988**, *4*, 921−937.

(19) Grundke, K.; Poschel, K.; Synytska, A.; Frenzel, R.; Drechsler, A.; Nitschke, M.; Cordeiro, A. L.; Uhlmann, P.; Welzel, P. B. Experimental Studies of Contact Angle Hysteresis Phenomena on Polymer Surfaces - toward the Understanding and Control of Wettability for Different Applications. *Adv. Colloid Interface Sci.* **2015**, *222*, 350−376.

(20) Sedev, R. V.; Petrov, J. G.; Neumann, A. W. Effect of Swelling of a Polymer Surface on Advancing and Receding Contact Angles. *J. Colloid Interface Sci.* **1996**, *180*, 36−42.

(21) Erbil, H. Y. The Debate on the Dependence of Apparent Contact Angles on Drop Contact Area or Three-Phase Contact Line: A Review. *Surf. Sci. Rep.* **2014**, *69*, 325−365.

(22) Podestà, A.; Fantoni, G.; Milani, P.; Guida, C.; Volponi, S. Nanotribological Characterization of Industrial Polytetrafluorethylene-Based Coatings by Atomic Force Microscopy. *Thin Solid Films* **2002**, *419*, 154−159.

(23) Perry, S. S.; Tysoe, W. T. Frontiers of Fundamental Tribological Research. *Tribol. Lett.* **2005**, *19*, 151−161.

(24) Myshkin, N. K.; Petrokovets, M. I.; Kovalev, A. V. Tribology of Polymers: Adhesion, Friction, Wear, and Mass-Transfer. *Tribol. Int.* **2005**, *38*, 910−921.

(25) Nuzzo, R. G.; Allara, D. L. Adsorption of Bifunctional Organic Disulfides on Gold Surfaces. *J. Am. Chem. Soc.* **1983**, *105*, 4481−4483.

(26) Telegdi, J.; Rigó, T.; Kálmán, E. Nanolayer Barriers for Inhibition of Copper Corrosion. *Corros. Eng., Sci. Technol.* **2004**, *39*, 65−70.

(27) Halik, M.; Klauk, H.; Zschieschang, U.; Schmid, G.; Dehm, C.; Schutz, M.; Maisch, S.; Effenberger, F.; Brunnbauer, M.; Stellacci, F.

Low-Voltage Organic Transistors with an Amorphous Molecular Gate Dielectric. *Nature* **2004**, *431*, 963−966.
(28) Maboudian, R.; Ashurst, W. R.; Carraro, C. Self-Assembled Monolayers as Anti-Stiction Coatings for MEMS: Characteristics and Recent Developments. *Sens. Actuators, A* **2000**, *82*, 219−223.
(29) Senaratne, W.; Andruzzi, L.; Ober, C. K. Self-Assembled Monolayers and Polymer Brushes in Biotechnology: Current Applications and Future Perspectives. *Biomacromolecules* **2005**, *6*, 2427−2448.
(30) Mir, M.; Alvarez, M.; Azzaroni, O.; Knoll, W. Comparison of Different Supramolecular Architectures for Oligonucleotide Biosensing. *Langmuir* **2008**, *24*, 13001−13006.
(31) Zheng, H.; Zhang, F.; Zhou, N.; Sun, M.; Li, X.; Xiao, Y.; Wang, S. Self-Assembled Monolayer-Modified ITO for Efficient Organic Light-Emitting Diodes: The Impact of Different Self-Assemble Monolayers on Interfacial and Electroluminescent Properties. *Org. Electron.* **2018**, *56*, 89−95.
(32) Smith, D. L.; Wysocki, V. H.; Colorado, R.; Shmakova, O. E.; Graupe, M.; Lee, T. R. Low-Energy Ion−Surface Collisions Characterize Alkyl- and Fluoroalkyl-Terminated Self-Assembled Monolayers on Gold. *Langmuir* **2002**, *18*, 3895−3902.
(33) Colorado, R.; Lee, T. R. Wettabilities of Self-Assembled Monolayers on Gold Generated from Progressively Fluorinated Alkanethiols. *Langmuir* **2003**, *19*, 3288−3296.
(34) Graupe, M.; Koini, T.; Wang, V. Y.; Nassif, G. M.; Colorado, R.; Villazana, R. J.; Dong, H.; Miura, Y. F.; Shmakova, O. E.; Lee, T. R. Terminally Perfluorinated Long-Chain Alkanethiols. *J. Fluorine Chem.* **1999**, *93*, 107−115.
(35) Frey, S.; Heister, K.; Zharnikov, M.; Grunze, M.; Tamada, K.; Colorado, R.; Graupe, M.; Shmakova, O. E.; Lee, T. R. Structure of Self-Assembled Monolayers of Semifluorinated Alkanethiols on Gold and Silver Substrates. *Isr. J. Chem.* **2000**, *40*, 81−97.
(36) Pujari, S. P.; Scheres, L.; Weidner, T.; Baio, J. E.; Stuart, M. A.; van Rijn, C. J.; Zuilhof, H. Covalently Attached Organic Monolayers onto Silicon Carbide from 1-Alkynes: Molecular Structure and Tribological Properties. *Langmuir* **2013**, *29*, 4019−4031.
(37) Barriet, D.; Chinwangso, P.; Lee, T. R. Can Cyclopropyl-Terminated Self-Assembled Monolayers on Gold Be Used to Mimic the Surface of Polyethylene? *ACS Appl. Mater. Interfaces* **2010**, *2*, 1254−1265.
(38) Fukushima, H.; Seki, S.; Nishikawa, T.; Takiguchi, H.; Tamada, K.; Abe, K.; Colorado, R.; Graupe, M.; Shmakova, O. E.; Lee, T. R. Microstructure, Wettability, and Thermal Stability of Semifluorinated Self-Assembled Monolayers (SAMs) on Gold. *J. Phys. Chem. B* **2000**, *104*, 7417−7423.
(39) Colorado, R., Jr; Lee, T. R. Physical Organic Probes of Interfacial Wettability Reveal the Importance of Surface Dipole Effects. *J. Phys. Org. Chem.* **2000**, *13*, 796−807.
(40) Bain, C. D.; Troughton, E. B.; Tao, Y. T.; Evall, J.; Whitesides, G. M.; Nuzzo, R. G. Formation of Monolayer Films by the Spontaneous Assembly of Organic Thiols from Solution onto Gold. *J. Am. Chem. Soc.* **1989**, *111*, 321−335.
(41) O'Hagan, D. Understanding Organofluorine Chemistry. An Introduction to the C-F Bond. *Chem. Soc. Rev.* **2008**, *37*, 308−319.
(42) Bondi, A. van der Waals Volumes and Radii. *J. Phys. Chem.* **1964**, *68*, 441−451.
(43) Zenasni, O.; Jamison, A. C.; Lee, T. R. The Impact of Fluorination on the Structure and Properties of Self-Assembled Monolayer Films. *Soft Matter* **2013**, *9*, 6356−6370.
(44) Chidsey, C. E. D.; Loiacono, D. N. Chemical Functionality in Self-Assembled Monolayers - Structural and Electrochemical Properties. *Langmuir* **1990**, *6*, 682−691.
(45) Zenasni, O.; Jamison, A. C.; Marquez, M. D.; Lee, T. R. Self-assembled monolayers on gold generated from terminally perfluorinated alkanethiols bearing propyl vs. ethyl hydrocarbon spacers. *J. Fluorine Chem.* **2014**, *168*, 128−136.
(46) Laibinis, P. E.; Whitesides, G. M.; Allara, D. L.; Tao, Y. T.; Parikh, A. N.; Nuzzo, R. G. Comparison of the Structures and Wetting Properties of Self-Assembled Monolayers of *N*-Alkanethiols on the Coinage Metal Surfaces, Copper, Silver, and Gold. *J. Am. Chem. Soc.* **1991**, *113*, 7152−7167.
(47) Vickerman, J. C.; Gilmore, I. S. *Surface Analysis− the Principal Techniques*, 2nd ed.; John Wiley & Sons: Chichester, 2009.
(48) Hutt, D. A.; Leggett, G. J. Influence of Adsorbate Ordering on Rates of UV Photooxidation of Self-Assembled Monolayers. *J. Phys. Chem.* **1996**, *100*, 6657−6662.
(49) Ishida, T.; Hara, M.; Kojima, I.; Tsuneda, S.; Nishida, N.; Sasabe, H.; Knoll, W. High Resolution X-Ray Photoelectron Spectroscopy Measurements of Octadecanethiol Self-Assembled Monolayers on Au(111). *Langmuir* **1998**, *14*, 2092−2096.
(50) Castner, D. G.; Hinds, K.; Grainger, D. W. X-Ray Photoelectron Spectroscopy Sulfur 2p Study of Organic Thiol and Disulfide Binding Interactions with Gold Surfaces. *Langmuir* **1996**, *12*, 5083−5086.
(51) Mancheno-Posso, P.; Muscat, A. J. Self-Assembly of Alkanethiolates Directs Sulfur Bonding with GaAs(100). *Appl. Surf. Sci.* **2017**, *397*, 1−12.
(52) Park, J. S.; Vo, A. N.; Barriet, D.; Shon, Y. S.; Lee, T. R. Systematic Control of the Packing Density of Self-Assembled Monolayers Using Bidentate and Tridentate Chelating Alkanethiols. *Langmuir* **2005**, *21*, 2902−2911.
(53) Colorado, R.; Lee, T. R. Attenuation Lengths of Photoelectrons in Fluorocarbon Films. *J. Phys. Chem. B* **2003**, *107*, 10216−10220.
(54) Zenasni, O.; Marquez, M. D.; Jamison, A. C.; Lee, H. J.; Czader, A.; Lee, T. R. Inverted Surface Dipoles in Fluorinated Self-Assembled Monolayers. *Chem. Mater.* **2015**, *27*, 7433−7446.
(55) Porter, M. D.; Bright, T. B.; Allara, D. L.; Chidsey, C. E. D. Spontaneously Organized Molecular Assemblies. 4. Structural Characterization of *N*-Alkyl Thiol Monolayers on Gold by Optical Ellipsometry, Infrared Spectroscopy, and Electrochemistry. *J. Am. Chem. Soc.* **1987**, *109*, 3559−3568.
(56) MacPhail, R. A.; Strauss, H. L.; Snyder, R. G.; Elliger, C. A. Carbon-Hydrogen Stretching Modes and the Structure of *N*-Alkyl Chains. 2. Long, All-Trans Chains. *J. Phys. Chem.* **1984**, *88*, 334−341.
(57) Snyder, R. G.; Strauss, H. L.; Elliger, C. A. Carbon-Hydrogen Stretching Modes and the Structure of *N*-Alkyl Chains. 1. Long, Disordered Chains. *J. Phys. Chem.* **1982**, *86*, 5145−5150.
(58) Liu, D.; He, Z.; Su, Y.; Diao, Y.; Mannsfeld, S. C. B.; Bao, Z.; Xu, J.; Miao, Q. Self-Assembled Monolayers of Cyclohexyl-Terminated Phosphonic Acids as a General Dielectric Surface for High-Performance Organic Thin-Film Transistors. *Adv. Mater.* **2014**, *26*, 7190−7196.
(59) Smallwood, I. M. *Handbook of Organic Solvent Properties*; John Wiley & Sons:: New York, 1996.
(60) Wohlfarth, C. Surface Tension of N-Methylformamide. In *Supplement to Iv/16*, Lechner, M. D., Ed.; Springer Berlin Heidelberg: Berlin, Heidelberg, 2008; pp 56−56.
(61) Fowkes, F. M.; Riddle, F. L.; Pastore, W. E.; Weber, A. A. Interfacial Interactions between Self-Associated Polar Liquids and Squalane Used to Test Equations for Solid Liquid Interfacial Interactions. *Colloids Surf.* **1990**, *43*, 367−387.
(62) Ewbank, J. D.; Kirsch, G.; Schafer, L. Electron-Diffraction Study of Hydrogen Isotope-Effects in Cyclohexane. *J. Mol. Struct.* **1976**, *31*, 39−45.
(63) Shon, Y. S.; Lee, S.; Colorado, R.; Perry, S. S.; Lee, T. R. Spiroalkanedithiol-Based SAMs Reveal Unique Insight into the Wettabilities and Frictional Properties of Organic Thin Films. *J. Am. Chem. Soc.* **2000**, *122*, 7556−7563.
(64) Aggarwal, S. L.; Sweeting, O. J. Polyethylene - Preparation, Structure, and Properties. *Chem. Rev.* **1957**, *57*, 665−742.

DOI: 10.1021/acsanm.9b01268
ACS Appl. Nano Mater. 2019, 2, 5809−5816